12-1-2005

Modeling, Parameter Identification, and Validation of Reactant and Water Dynamics for a Fuel Cell Stack

D. A. McKay
University of Michigan, Ann Arbor, dmckahn@smith.edu

W. T. Ott
University of Michigan, Ann Arbor

A. G. Stefanopoulou
University of Michigan, Ann Arbor

Recommended Citation

IMECE2005-81484

MODELING, PARAMETER IDENTIFICATION, AND VALIDATION OF REACTANT AND WATER DYNAMICS FOR A FUEL CELL STACK

D. A. McKay, W. T. Ott, A. G. Stefanopoulou,

Fuel Cell Control Laboratory[*]
Department of Mechanical Engineering
University of Michigan, Ann Arbor, MI 48109
Email: annastef@umich.edu

ABSTRACT

This paper describes a simple two-phase flow dynamic model that predicts the experimentally observed temporal behavior of a proton exchange membrane fuel cell stack and a methodology to experimentally identify tunable physical parameters. The model equations allow temporal calculation of the species concentrations across the gas diffusion layers, the vapor transport across the membrane, the degree of flooding in the electrodes, and then predict the resulting decay in cell voltage over time. A nonlinear optimization technique is used for the identification of two critical model parameters, namely the membrane water vapor diffusion coefficient and the thickness of the liquid water film covering the fuel cell active area. The calibrated model is validated for a 24 cell, 300 cm^2 stack with a supply of pressure regulated pure hydrogen.

1 Introduction

The management of water within the fuel cell stack is critical for optimal stack performance. Because the ionic conductivity of the membrane is dependent upon its water content, a balance must be struck between reactant delivery, namely hydrogen and oxygen, and water supply and removal. When the reactant gases become saturated, excess water will condense. This liquid water can accumulate in the gas channels, the pore space of the gas diffusion layer (GDL), or can partially coat the catalyst, reduc-

ing the number of catalyst sites available (effective area), in turn reducing the power output of the fuel cell.

Numerous studies have investigated the formation of liquid water droplets within the cell layers by use of translucent cells with optical sensors [1, 2] or neutron imaging [3]. While useful for understanding and characterizing droplet formation dynamics in the GDL, multi-cell stacks can not be easily examined using these experimental techniques. Many CFD models have been developed to approximate the 2 or 3 dimensional flow of hydrogen, air, and water within the manifolds, gas channels, and GDL [4–7]. These models are ideal for investigating fuel cell design issues, however, implementation of such complex models for real time embedded control is cumbersome. Thus, any model based control scheme used for water management must adequately trade-off implementation while still capturing the dynamic behavior of electrode flooding and two phase flow.

Due to the difficulty of measuring the humidity or water content within the diffusion layers or gas channels, a low order model is developed to quantify the liquid water saturation and rate of condensation in the GDL. These GDL dynamics are added to an existing lumped parameter low order fuel cell model, [8], capturing the water and reactant dynamics within the cell. This work previously lumped the gas diffusion and catalyst layers into a single volume and neglected the effects associated with the formation of liquid water. The addition of the liquid water and gas dynamics within the GDL is a necessary step to afford the simulation of flooding (the effect that liquid water has in restricting the diffusion of reactant gas to the catalyst and thus lowering the

cell voltage). The methodology used to experimentally identify tunable parameters is described. Finally, experimental data will be compared to the model predictions to provide a validation of the models presented. This is the first time to our knowledge that a two-phase flow, 1-D model predicts the experimentally observed temporal behavior of a multi-cell stack.

Note, this work spatially discretizes the GDL and not the membrane. The intent of this work is to model the reactant dynamics within each electrode, and their impact on cell performance. It can be assumed that reactant gases do not penetrate the membrane, thus no reactant gases are contained within the membrane. Additionally, the spatial variation of water vapor in the membrane is neglected due to the significant difference in thickness between the GDL (432 μm) and the membrane (35 μm). Thus, the membrane is considered to be homogenous and lumped parameter.

2 Nomenclature

Time derivatives are denoted as $d(\ )/dt$. Spatial derivatives through the GDL thickness in the membrane direction (y) are denoted as $\partial(\ )/\partial y$.

The English letter a denotes water activity, A_{fc} is the fuel cell active area (m^2), c is molar concentration (mol/m^3), D is diffusion coefficient (m^2/s), $\langle D \rangle$ is the effective diffusivity (m^2/s), i is current density (A/cm^2), I is current (A), K is absolute permeability (m^2), K_{rl} is relative permeability, M is molecular weight (kg/mole), n is the mole number, n_{cells} is the number of cells in the stack, N is molar flux (mol/s/m^2), p is pressure (Pa), R is the ideal gas constant (J/kg K), R_{evap} is the evaporation rate (mol/s m^3), s is the fraction of liquid water volume to the total volume, s_{im} is the level of immobile saturation, S is the reduced liquid water saturation, t_{mb} is the membrane thickness (m), t_{wl} is the tunable water layer thickness parameter (m), T is temperature (K), u is voltage (V), V is volume (m^3), W is the mass flow (kg/s), x is molar ratio, y is mass ratio, and z is the ratio of molar fluxes. The Greek letter α_w is the tunable diffusion parameter, γ is used for the volumetric condensation coefficient (s^{-1}), ε for porosity, θ_c is contact angle (degrees), λ for water content, μ for viscosity (kg/m s), ρ for density (kg/m^3), σ is surface tension (N/m), ϕ for relative humidity (0-1), and ω for humidity ratio.

The subscript an denotes variables associated with the anode, c is capillary, ca is cathode, ch is channel, ct is catalyst, da is dry air, e is electrode (an or ca), gas is the gas constituent, H_2 is hydrogen, in is into the control volume, j is used as an index for gas constituents, k is used as an index for discretization, l is liquid, mb is membrane, N_2 is nitrogen, O_2 is oxygen, out is out of the control volume, p is pore, rc is reactions, sat is saturation, st is stack, w is water, and v is vapor.

3 Model Overview

Figure 1 shows a flow chart of the calculation algorithm used to implement the model. In the anode channel, a mixture of hy-
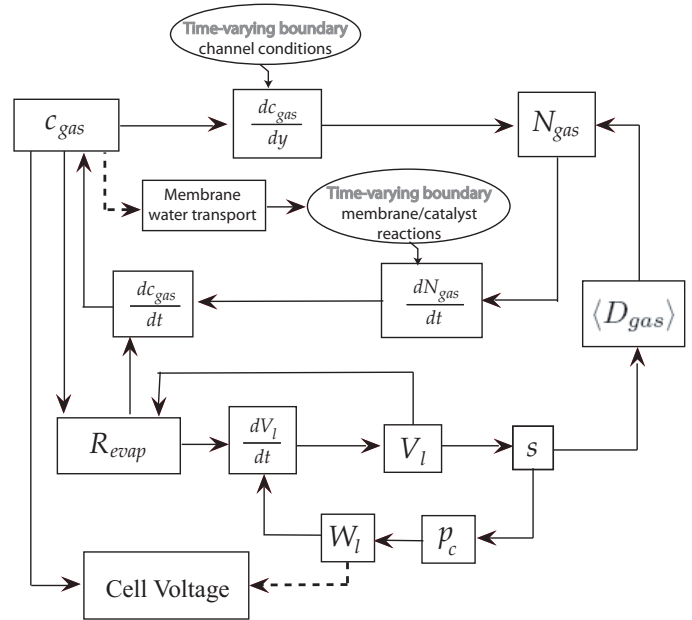

Figure 1. Flow chart of model calculation algorithm

drogen and water vapor flow through the GDL. In the cathode channel a mixture of oxygen, nitrogen, and water vapor are flowing. The species concentrations in the channel are calculated based on conservation of mass assuming the channel is homogeneous, lumped-parameter, and isothermal. The time varying channel concentrations provide one set of boundary conditions for the spatially varying reactant diffusion through the GDL. The reactant gases must diffuse through the GDL to reach the catalytic layer.

Under load, we assume product water is formed as a vapor. The combination of electro-osmotic drag and back diffusion transport vapor throught the membrane, between the anode and cathode. The protons, liberated at the anode, transport water to the cathode through electro-osmosis, while back diffusion transfers vapor due to a water vapor concentration gradient. The net flux of vapor through the membrane depends on the relative magnitudes diffusion and drag. Although there are many efforts to quantify back diffusion ([9], [10], [11]), conflicting results suggest an empirically data-driven identification of water vapor diffusion might be a practical approach to this elusive subject. The membrane water transport algorithm, thus, depends on an unknown tunable parameter (indicated by a dashed line in Figure 1) that scales the diffusion model in [10].

The diffusive migration of gases and capillary flow of liquid water through the GDL are modeled using a diffusion coefficient, which depends on the local saturation of liquid water [12]. The condensation rate of vapor is modeled through a discretization of the GDL [13]. Under isothermal conditions, when the production or transport of vapor overcomes the ability of the vapor to diffuse

through the GDL to the channel, the vapor supersaturates and condenses. The condensed liquid accumulates in the GDL until it has surpassed the immobile saturation limit at which point capillary flow will carry it to an area of lower capillary pressure (the GDL-channel interface). Liquid water in the GDL occupies pore space, reducing the effective area through which reactant gas can diffuse and increasing the tortuosity of the diffusion path. This obstruction ultimately reduces the active catalyst surface area, in turn lowering the cell voltage at a fixed current. This effect is not easily modeled because the surface roughness makes it difficult to predict how much GDL surface area is blocked by a given volume of water. For this reason, we chose to experimentally identify the thickness of the liquid that determines the area blocked by the liquid water flowing out of the GDL. The location of this second tunable parameter within the overall model calculations is indicated with the second dashed line in Figure 1.

4 Gas Diffusion Layer

The diffusion of gas species in the diffusion layer is a function of the concentration gradient, transferring gas from regions of higher concentration to regions of lower concentration. The molar concentration of gas species j is denoted c_j and is a function of n_j (the number of moles of gas j in pore volume V_p):

$$c_j = \frac{n_j}{V_p} = \frac{p_j}{RT} .$$ (1)

The time derivatives of gas concentrations for two general gas species A and B are a function of the local molar flux gradients (∇N_A and ∇N_B), and the local reaction rates R_A and R_B of the particular gas species (as in the case of vapor condensation) forming two partial differential equations (PDEs):

$$\frac{dc_A}{dt} = \nabla N_A + R_A = \frac{\partial N_A}{\partial y} + R_A ,$$ (2a)

$$\frac{dc_B}{dt} = \nabla N_B + R_B = \frac{\partial N_B}{\partial y} + R_B .$$ (2b)

Diffusion in the GDL occurs between hydrogen and vapor in the anode, and oxygen and vapor in the cathode (nitrogen diffusion is not considered). We present first the general equations of diffusion in two phase flow. The exact time varying diffusion equations are given in Section 4.4.

4.1 Gas Species Diffusion

Gas flow is calculated in units of molar flux, which measures the molar flow rate through a cross sectional area in units of mol/s/m^2. The gas molar flux accounts for both the diffusive molar flux and the convective molar flux. The diffusive molar flux is caused by a concentration gradient, as shown in Figure 2 for a non-equilibrium distribution of gases A and B. The concentration
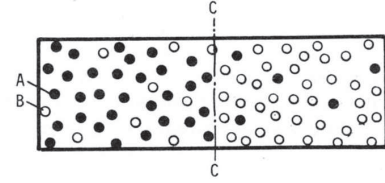

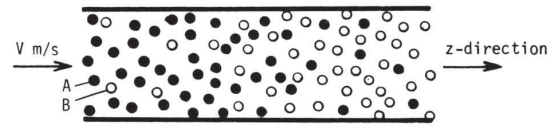Figure 2.   Molecules A and B confined in a box [14]

Figure 3.   Mixture of A and B with bulk velocity V and concentration gradients [14]

gradient is diffusion's driving force. Molecular diffusion causes species A to move to the right and B to move to the left, towards the respective direction of decreasing concentration according to Fick's law. Fickian diffusion is represented by $-D_{AB}\frac{\partial c_A}{\partial y}$, where D_{AB} is the diffusion coefficient of gas A with respect to gas B. Similarly, the diffusive flux for gas B is: $-D_{BA}\frac{\partial c_B}{\partial y}$.

For two gases diffusing in a mixture with a bulk (convective) flow, shown in Figure 3, we first define the molar ratio of gas species j being $x_j = c_j/c$ and the average gas velocity $\bar{V} = (N_A + N_B)/c$. Then the total molar flux is a function of the average gas velocity, $x_j c \bar{V}$, and the diffusive flux, described by:

$$N_A = -D_{AB}\frac{\partial c_A}{\partial y} + x_A(N_A + N_B) ,$$ (3a)

$$N_B = -D_{BA}\frac{\partial c_B}{\partial y} + x_B(N_A + N_B) .$$ (3b)

To solve these equations, we assume a ratio between N_A and N_B, $z = \frac{N_B}{N_A}$ that changes gradually in space as shown later in Equations (11) and (12).

4.2 Effective diffusivity

The effective diffusivity of gas constituents in the GDL, $\langle D_j \rangle$, is a function of the porosity of the diffusion layer, ε, as well as the volume of liquid water present, V_l:

$$\langle D_j \rangle = D_j \varepsilon \left(\frac{\varepsilon - 0.11}{1 - 0.11}\right)^{0.785} (1 - s)^2, \qquad s = \frac{V_l}{V_p} ,$$ (4)

where s is the liquid water saturation ratio, and V_p is the pore volume of the diffusion layer [12]. The porosity of the diffusion

layer is the ratio of the pore volume to the total volume of the layer, $\varepsilon = V_p/V$. Both the impact of liquid water saturation on effective diffusivity and the impact of porosity for carbon Toray^R paper GDL, described here, was modeled in [12].

4.3 Liquid Water Capillary Transport

The volume of liquid water in the GDL is calculated through the capillary liquid water flow, W_l, and the evaporation rate, R_{evap}:

$$\rho_l \frac{dV_l}{dt} = W_{l,in} - W_{l,out} - \frac{R_{evap}V_p M_v}{\varepsilon} \quad . \tag{5}$$

As a pore fills with liquid water, the capillary pressure increases, causing the water to flow to an adjacent pore with less water. This process creates a flow of liquid water through the GDL, resulting in the injection of liquid into the channel (shown in Figure 4). This liquid water flow through the GDL is a function of the capillary pressure gradient [12, 15],

$$W_l = -\frac{A_{fc} n_{cells} \rho_l K K_{rl}}{\mu_l} \left(\frac{dp_c}{dS}\right)\left(\frac{\partial S}{\partial y}\right) , \tag{6}$$

where p_c is capillary pressure, A_{fc} is the fuel cell active area, n is the number of cells, ρ_l is the liquid water density, K is the absolute permeability, μ_l is the viscosity of liquid water, $K_{rl} = S^3$ is the relative permeability of liquid water, and S is the reduced water saturation,

$$S = \begin{cases} \frac{s - s_{im}}{1 - s_{im}} & \text{for } s_{im} < s \leq 1 \\ 0 & \text{for } 0 \leq s \leq s_{im} \end{cases} \quad . \tag{7}$$

Here, s_{im} is the level of immobile saturation describing the point at which the liquid water becomes discontinuous and interrupts capillary flow. Capillary flow is interrupted when $s < s_{im}$. The results of capillary flow experiments using glass beads as porous media show that $s_{im} = 0.1$ [12]. The relative permeability function suggests more pathways for capillary flow are available as liquid saturation increases.

Capillary pressure is the surface tension of the water droplet integrated over the surface area. The Leverette J-function describes the relationship between capillary pressure and the reduced water saturation:

$$p_c = \frac{\sigma \cos \theta_c}{(K/\varepsilon)^{\frac{1}{2}}} \underbrace{\left[1.417S - 2.120S^2 + 1.263S^3\right]}_{J(S)} , \tag{8}$$

where σ is the surface tension between water and air, and θ_c is the contact angle of the water droplet.

Finally, the molar evaporation rate based on [12] is

$$R_{evap} = \gamma \frac{p_{v,sat} - p_v}{RT} , \quad p_v = c_v RT , \tag{9}$$

where γ is the volumetric condensation coefficient. When the partial pressure of vapor is greater than the saturation pressure, R_{evap} is negative, representing the condensation of water. A logical constraint must be included such that if no liquid water is present, $R_{evap} \leq 0$.
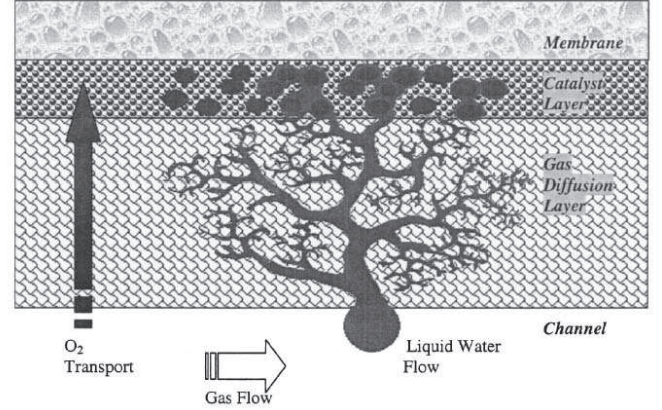

Figure 4. Capillary flow of liquid water through diffusion layer [12]

4.4 Details on discretization of the spatial gradients

The mass transport of gas and liquid water can be more easily solved when the gas diffusion layer is split into discrete volumes (refer to Figure 5). Each sub-volume in the diffusion layer is assumed to be homogenous. The spatial gradients are solved as difference equations, while the time derivatives are solved with classical ODE solvers. For the purposes of model simplification, the concentration of nitrogen in the cathode diffusion layer is assumed to be identical to the concentration in the channel, as nitrogen is not consumed in the chemical reaction. Generally, the concentration gradients are:

Cathode Equations	Anode Equations
$\frac{\partial \psi}{\partial y}(1) = \frac{\psi(2) - \psi(1)}{\delta y}$	$\frac{\partial \psi}{\partial y}(1) = \frac{\psi(1) - \psi(2)}{\delta y}$
$\frac{\partial \psi}{\partial y}(2) = \frac{\psi(3) - \psi(2)}{\delta y}$	$\frac{\partial \psi}{\partial y}(2) = \frac{\psi(2) - \psi(3)}{\delta y}$
$\frac{\partial \psi}{\partial y}(3) = \frac{\psi_{ch} - \psi(3)}{0.5\delta y}$	$\frac{\partial \psi}{\partial y}(3) = \frac{\psi(3) - \psi_{ch}}{0.5\delta y}$

$$(10)$$

where ψ is used to denote the variable of interest. For the cathode, difference equations are used to describe the concentration of oxygen, c_{O_2}, vapor, $c_{v,ca}$, and reduced water saturation, S_{ca}. For the anode, difference equations are used to describe the concentration of hydrogen, c_{H_2}, vapor, $c_{v,an}$, and reduced water saturation, S_{an}.

The ratio of molar flux is a function of the gas concentration gradient, and the effective diffusion rate. The resulting cathode equations are as follows:

$$z_{ca}(k) = \begin{cases} N_{v,ct}/N_{O_2,rct} & \text{for k=1} \\ N_{v,ca}(k-1)/N_{O_2}(k-1) & \text{for k=2,3} \end{cases} \tag{11a}$$

$$N_{O_2}(k) = \frac{-\langle D_{O_2}(k)\rangle}{1 - x_{O_2}(k)(1 + z_{ca}(k))} \frac{\partial c_{O_2}}{\partial y}(k) \tag{11b}$$

$$N_{v,ca}(k) = \frac{-\langle D_{v,ca}(k)\rangle}{1 - x_{v,ca}(k)(1 + 1/z_{ca}(k))} \frac{\partial c_{v,ca}}{\partial y}(k) \tag{11c}$$

where $N_{v,ct} = N_{v,rct} + N_{v,mb}$ and $N_{v,mb}$ are defined in (21). Simi-
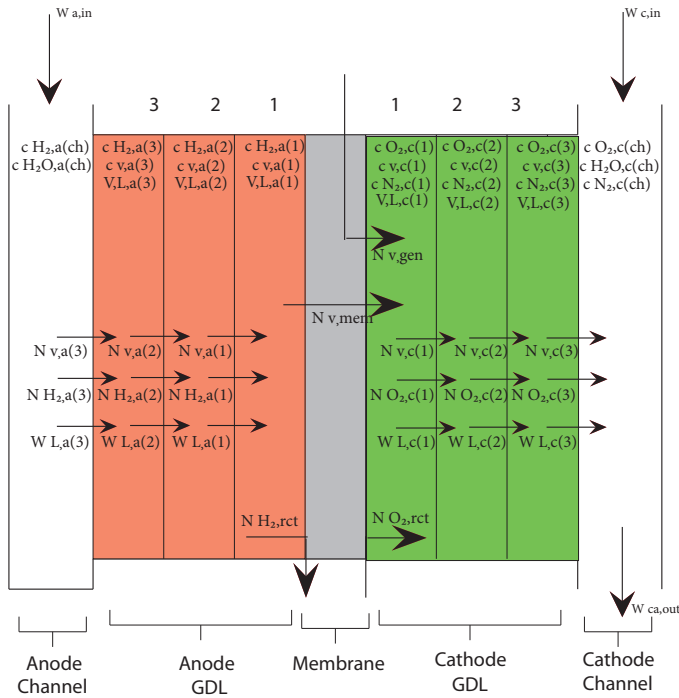
Figure 5. Mass Transport Diagram with discretization of diffusion layer

larly, the anode equations are as follows:

$$z_{an}(k) = \begin{cases} N_{v,mb}/N_{H_2,rct} & \text{for k=1} \\ N_{v,an}(k-1)/N_{H_2}(k-1) & \text{for k=2,3} \end{cases} \quad (12a)$$

$$N_{H_2}(k) = \frac{-\langle D_{H_2}(k)\rangle}{1-x_{H_2}(k)(1+z_{an}(k))}\frac{\partial c_{H_2}}{\partial y}(k) \quad (12b)$$

$$N_{v,an}(k) = \frac{-\langle D_{v,an}(k)\rangle}{1-x_{v,an}(k)(1+1/z_{an}(k))}\frac{\partial c_{v,an}}{\partial y}(k) \quad (12c)$$

The molar flux gradients of oxygen and hydrogen are:

Cathode Equations	Anode Equations
$\frac{\partial N_{O_2}}{\partial y}(1) = \frac{N_{O_2}(1)-N_{O_2,rct}}{\delta y}$	$\frac{\partial N_{H_2}}{\partial y}(1) = \frac{N_{H_2,rct}-N_{H_2}(1)}{\delta y}$
$\frac{\partial N_{O_2}}{\partial y}(2) = \frac{N_{O_2}(2)-N_{O_2}(1)}{\delta y}$	$\frac{\partial N_{H_2}}{\partial y}(2) = \frac{N_{H_2}(1)-N_{H_2}(2)}{\delta y}$
$\frac{\partial N_{O_2}}{\partial y}(3) = \frac{N_{O_2}(3)-N_{O_2}(2)}{\delta y}$	$\frac{\partial N_{H_2}}{\partial y}(3) = \frac{N_{H_2}(2)-N_{H_2}(3)}{\delta y}$

(13)

and the molar flux gradients of water vapor are:

Cathode Equations	Anode Equations
$\frac{\partial N_{v,ca}}{\partial y}(1) = \frac{N_{v,ca}(1)-N_{v,ct}}{\delta y}$	$\frac{\partial N_{v,an}}{\partial y}(1) = \frac{N_{v,mb}-N_{v,an}(1)}{\delta y}$
$\frac{\partial N_{v,ca}}{\partial y}(2) = \frac{N_{v,ca}(2)-N_{v,ca}(1)}{\delta y}$	$\frac{\partial N_{v,an}}{\partial y}(2) = \frac{N_{v,an}(1)-N_{v,an}(2)}{\delta y}$
$\frac{\partial N_{v,ca}}{\partial y}(3) = \frac{N_{v,ca}(3)-N_{v,ca}(2)}{\delta y}$	$\frac{\partial N_{v,an}}{\partial y}(3) = \frac{N_{v,an}(2)-N_{v,an}(3)}{\delta y}$

(14)

The time derivatives describing the dependance of the gas concentrations on the molar flux gradients for the cathode are:

$$\frac{dc_{O_2}}{dt}(k) = -\frac{\partial N_{O_2}}{\partial y}(k), \quad (15a)$$

$$\frac{dc_{v,ca}}{dt}(k) = -\frac{\partial N_{v,ca}}{\partial y}(k)+R_{evap,ca}(k). \quad (15b)$$

Similarly for the anode:

$$\frac{dc_{H_2}(k)}{dt} = -\frac{\partial N_{H_2}}{\partial y}(k), \quad (16a)$$

$$\frac{dc_{v,an}(k)}{dt} = -\frac{\partial N_{v,an}}{\partial y}(k)+R_{evap,an}(k). \quad (16b)$$

The electrode water evaporation rate, $R_{evap,e}$, is a function of the partial pressure of water vapor in the electrode, $p_{v,e}$, and the vapor saturation pressure, $p_{v,sat}$, which itself is a function of temperature:

$$R_{evap,e}(k) = \gamma\frac{p_{v,sat}(T)-p_{v,e}(k)}{RT}. \quad (17)$$

The time derivatives of liquid water volume are a function of the evaporation rate, and the liquid water mass flow, expressed for the cathode and anode as:

$$\frac{dV_{l,ca}}{dt}(k) = \begin{cases} \frac{-\frac{V_pM_v}{\varepsilon}R_{evap,ca}(k)-W_{l,ca}(k)}{\rho_l} & \text{for k=1} \\ \frac{-\frac{V_pM_v}{\varepsilon}R_{evap,ca}(k)+W_{l,ca}(k-1)-W_{l,ca}(k)}{\rho_l} & \text{for k=2,3} \end{cases} \quad (18a)$$

$$\frac{dV_{l,an}}{dt}(k) = \begin{cases} \frac{-\frac{V_pM_v}{\varepsilon}R_{evap,an}(k)+W_{l,an}(k)}{\rho_l} & \text{for k=1} \\ \frac{-\frac{V_pM_v}{\varepsilon}R_{evap,an}(k)-W_{l,an}(k-1)-W_{l,an}(k)}{\rho_l} & \text{for k=2,3} \end{cases} \quad (18b)$$

where the mass flow of liquid water from (6) is a function of the reduced water saturation gradient and the capillary pressure, p_c, written generally for the electrode as:

$$W_{l,e}(k) = -\frac{A_{fc}n_{cells}\rho_l K K_{rl,e}(k)}{\mu_l}\frac{dp_c}{dS}(k)\frac{\partial S_e}{\partial y}(k). \quad (19)$$

5 Boundary conditions at the membrane

The reaction at the catalyst surface of the membrane used in the calculation of the molar flux gradient in Equations (13) and (14) are:

$$N_{(\,),rct} = \frac{I_{st}}{2\xi F} \text{ with } \begin{cases} \xi = 1 \text{ for } H_2 \text{ and } H_2O \\ \xi = 2 \text{ for } O_2 \end{cases} \quad (20)$$

where I_{st} is the current drawn from the stack and F is the Faraday constant.

The water content of the membrane and the water vapor flow rate across the membrane are calculated. These properties are assumed to be invariant across the membrane surface. The mass flux, $N_{v,mb}$, of vapor across the membrane in Equation (14) is calculated using mass transport principles and membrane properties given in [10] according to:

$$N_{v,mb} = n_d\frac{i}{F} - \alpha_w D_w\frac{(c_{v,ca,mb}-c_{v,an,mb})}{t_{mb}}, \quad (21)$$

5

where i is the fuel cell current density (I_{st}/A_{fc}), n_d is the electro-osmotic drag coefficient, D_w is the membrane vapor diffusion coefficient, and t_{mb} is the membrane thickness. The parameter α_w is identified using experimental data. The water concentration in the electrode is:

$$c_{v,e,mb} = \frac{\rho_{mb,dry}}{M_{mb,dry}}\lambda_e \qquad (22)$$

where $\rho_{mb,dry}$ is the membrane dry density and $M_{mb,dry}$ is the membrane dry equivalent weight. The membrane water content, λ_j, defined as the ratio of water molecules to the number of charge sites [10], is calculated from water activities a_j (where subscript j is either an-anode, ca-cathode, or mb-membrane),

$$\lambda_j = \begin{cases} 0.043 + 17.81a_j - 39.85a_j^2 + 36.0a_j^3, & 0 < a_j \leq 1 \\ 14 + 1.4(a_j - 1), & 1 < a_j \leq 3 \\ 16 & \text{elsewhere} \end{cases} \quad (23)$$

where the average water activity, a_{mb}, between the anode and cathode water activities, is described by:

$$a_{mb} = \frac{a_{an,mb} + a_{ca,mb}}{2} \quad \text{and} \quad a_{e,mb} = \frac{x_{w,e}(1)p_e(1)}{p_{sat,e}} , \qquad (24)$$

with $p_e(1)$ being the total gas pressure in the GDL layer next to the membrane, calculated using the concentration defined in Equations (15) and (16). The membrane vapor diffusion coefficient presented by [6] is a piecewise linear approximation of the data published by [10]:

$$D_w = D_\lambda exp\left(2416\left(\frac{1}{303} - \frac{1}{T_{st}}\right)\right) \qquad (25)$$

$$D_\lambda = \begin{cases} 10^{-10} & ,\lambda < 2 \\ 10^{-10}(1 + 2(\lambda - 2)) & ,2 \leq \lambda \leq 3 \\ 10^{-10}(3 - 1.67(\lambda - 3)) & ,3 < \lambda < 4.5 \\ 1.25 \cdot 10^{-10} & ,\lambda \geq 4.5 \end{cases}$$

where D_λ is the corrected diffusion coefficient (m^2/s). Finally, the electro-osmotic drag coefficient is described by [6] is calculated using:

$$n_d = 0.0029\lambda_{mb}^2 + 0.05\lambda_{mb} - 3.4x10^{-19} . \qquad (26)$$

6 Boundary conditions at the cathode channel

The concentration of reactants and vapor in the anode and cathode channel are used for the calculations of the gas concentration gradient in the last GDL layer (next to the channels) in Equation (10). Mass conservation for the gas species in the cathode is applied using the cathode inlet conditions as inputs, requiring measurements of the dry air mass flow rate $W_{da,ca,in}$, temperature $T_{ca,in}$ (is assumed to be T_{st}), pressure $p_{ca,in}$ (is calculated using the stack back pressure-flow characteristic $f(W_{da,ca,in})$), and humidity $\phi_{ca,in}$ (is assumed to be 1), along with the cathode outlet pressure $p_{ca,out}$ (is assumed to be ambient p_{atm}). These assumptions have been experimentally confirmed.

The mass flow of the individual gas species supplied to the cathode channel are calculated as follows:

$$\begin{aligned} W_{O_2,ca,in} &= y_{O_2,ca,in}\frac{1}{1 + \omega_{ca,in}}W_{da,ca,in}, \\ W_{N_2,ca,in} &= y_{N_2,ca,in}\frac{1}{1 + \omega_{ca,in}}W_{da,ca,in}, \\ W_{v,ca,in} &= \frac{\omega_{ca,in}}{1 + \omega_{ca,in}}W_{da,ca,in}. \end{aligned} \qquad (27)$$

where

$$\omega_{ca,in} = \frac{M_v}{M_{da}^{atm}}\frac{\phi_{ca,in}p_{sat}(T_{ca,in})}{p_{ca,in} - \phi_{ca,in}p_{sat}(T_{ca,in})}. \qquad (28)$$

with the mass fraction of oxygen and nitrogen in the dry air (da) as $y_{O_2,ca,in} = x_{O_2}M_{O_2}/M_{da}^{atm}$ and $y_{N_2,ca,in} = (1 - x_{O_2})M_{N_2}/M_{da}^{atm}$, where $M_{da}^{atm} = x_{O_2}M_{O_2} + (1 - x_{O_2})M_{N_2}$ and $x_{O_2} = 0.21$ is the oxygen mole fraction in dry air.

The mass of gas species in the cathode channel are balanced by applying mass continuity:

$$\begin{aligned} \frac{dm_{O_2,ca,ch}}{dt} &= W_{O_2,ca,in} - W_{O_2,ca,out} - W_{O_2,ca,GDL}, \\ \frac{dm_{N_2,ca,ch}}{dt} &= W_{N_2,ca,in} - W_{N_2,ca,out}, \\ \frac{dm_{w,ca,ch}}{dt} &= W_{v,ca,in} - W_{v,ca,out} + W_{w,ca,GDL}. \end{aligned} \qquad (29)$$

The mass of water is in vapor form until the relative humidity of the gas reaches saturation (100%), at which point vapor condenses into liquid water. The cathode pressure is calculated using Dalton's law of partial pressures $p_{ca,ch} = p_{O_2,ch} + p_{N_2,ch} + p_{v,ca,ch}$. Note also that the partial pressures for the oxygen $p_{O_2,ch} = \frac{RT_{st}}{M_{O_2}V_{ca}}m_{O_2,ch}$, nitrogen $p_{N_2,ch} = \frac{RT_{st}}{M_{N_2}V_{ca}}m_{N_2,ch}$, and vapor $p_{v,ca,ch} = \phi_{ca,ch}p_{sat}(T_{st})$ in the cathode are algebraic functions of the states through the ideal gas law and the psychrometric properties since the cathode temperature is assumed to be fixed and equal to the overall stack temperature at T_{st}. Given the vapor saturation pressure $p_{sat}(T_{st})$, the relative humidity in the gas channel is $\phi_{ca,ch} = \min\left[1, \frac{m_{w,ca,ch}RT_{st}}{p_{sat}(T_{st})M_vV_{ca}}\right]$. Although the cathode airflow may be responsible for removing some liquid water, it is assumed that all water exiting the cathode is in the form of vapor.

The mass flow rate of gases exiting the cathode are calculated as:

$$\begin{aligned} W_{ca,out} &= k_{ca}(p_{ca,ch} - p_{ca,out}), \\ W_{O_2,ca,out} &= \frac{m_{O_2,ca,ch}}{m_{ca}}W_{da,ca,out}, \\ W_{N_2,ca,out} &= \frac{m_{N_2,ca,ch}}{m_{ca}}W_{da,ca,out}, \\ W_{v,ca,out} &= \frac{p_{v,ca,ch}V_{ca}M_v}{RT_{st}m_{ca,ch}}W_{da,ca,out}, \end{aligned} \qquad (30)$$

where k_{ca} is an orifice constant found experimentally, and $m_{ca,ch} = m_{O_2,ca,ch} + m_{N_2,ca,ch} + p_{v,ca,ch}V_{ca}M_v/(RT_{st})$ is the total mass of the cathode gas. Finally, the oxygen diffused to the GDL is calculated using Equation (11) and the water (vapor and liquid) flowing from the GDL is calculated using Equations (11) and (19):

$$W_{O_2,ca,GDL} = N_{O_2}(3)M_{O_2}A_{fc}n_{cells},$$
$$W_{w,ca,GDL} = W_{l,ca}(3) + N_{v,ca}(3)M_v A_{fc}n_{cells} . \qquad (31)$$

At the surface of the GDL adjacent to the channel, $S = 0$. This boundary condition is used in the reduced water saturation gradient equation, causing the capillary pressure to be zero at the GDL surface. The reduced water saturation is calculated for each element using Equations 7 and 4.

7 Boundary conditions at the anode channel

Similarly, the inputs for the anode calculations are the measured anode inlet conditions of dry hydrogen mass flow $W_{H_2,an,in}$, temperature $T_{an,in}$ (assume T_{st}), supply manifold pressure $p_{an,in}$, relative humidity $\phi_{an,in}$ (zero humidity is assumed), and outlet manifold pressure $p_{an,out}$ (assumed to be ambient p_{atm}). The dry hydrogen inlet mass flow rate $W_{H_2,an,in} = k_{an,in}(p_{an,in} - p_{an})$ is manually regulated to maintain a constant anode inlet pressure. The hydrogen supplied to the anode is dry, therefore $W_{v,an,in} = 0$. The mass balances for hydrogen and water are

$$\frac{dm_{H_2,an,ch}}{dt} = W_{H_2,an,in} - W_{H_2,an,out} - W_{H_2,an,GDL},$$
$$\frac{dm_{w,an,ch}}{dt} = W_{v,an,in} - W_{v,an,out} - W_{w,an,GDL}, \qquad (32)$$

with the anode pressure and relative humidity calculated as

$$p_{an,ch} = \underbrace{\frac{RT_{st}}{M_{H_2}V_{an}}m_{H_2}}_{p_{H_2,an,ch}} + \underbrace{\min\left[1, \frac{RT_{st}m_{w,an}}{M_v V_{an}p_{sat}(T_{st})}\right]}_{\phi_{an,ch}}p_{sat}(T_{st}).$$

The anode exit flow rate, $W_{an,out} = k_{an,out}(p_{an,ch} - p_{an,out})$, represents the purge of anode gas to remove both water, and unfortunately, hydrogen:

$$W_{H_2,an,out} = \frac{m_{H_2,an,ch}}{m_{an}}W_{an,out},$$
$$W_{v,an,out} = \frac{p_{v,an,ch}V_{an}M_v}{RT_{st}m_{an,ch}}W_{an,out}. \qquad (33)$$

where $m_{an,ch} = m_{H_2,an,ch} + p_{v,an,ch}V_{an}M_v/(RT_{st})$. The hydrogen and vapor diffused to the GDL are calculated using Equations (12) and (19):

$$W_{H_2,an,GDL} = N_{H_2}(3)M_{H_2}A_{fc}n_{cells},$$
$$W_{w,an,GDL} = W_{l,an}(3) + N_{v,an}(3)M_v A_{fc}n_{cells}. \qquad (34)$$

8 Experimental Set-up

The experimental data used to calibrate and validate our model are taken at the Fuel Cell Control Laboratory at the University of Michigan. A computer controlled system coordinates air, hydrogen, cooling, and electrical subsystems to operate the PEMFC stack. Dry pure hydrogen is pressure regulated to replenish the hydrogen consumed in the chemical reaction. The hydrogen stream is dead ended with no flow external to the anode. Using a purge solenoid valve, hydrogen is momentarily purged through the anode to remove condensed water accumulating in the gas diffusion layers and flow channels. Humidified air is flow controlled, in excess of the reaction rate, to provide a supply of water vapor and oxygen at the cathode. Deionized water is circulated through the system to remove heat produced due to the exothermic chemical reaction.

Measurements of dry gas mass flow delivered to the electrodes are taken along with the electrode inlet and outlet temperature, pressure and relative humidity. The coolant temperature is measured leaving the cells. Figure 6, displays the major experimental components along with the measurement locations.
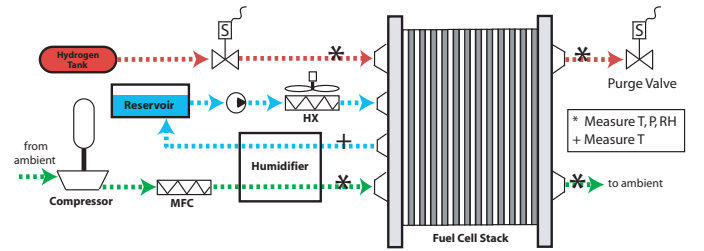

Figure 6.   Experimental hardware and measurement locations

A 24-cell PEMFC stack was used for all experimental results presented. The stack delivers 1.4 kW continuous power, capable of peaking to 2.5 kW. The cell membranes are comprised of GORE^{TM} PRIMEA^R Series 5620 membrane electrode assemblies (MEAs). The MEAs utilize 35 μm thick membranes with microporous layers containing 0.4 mg/cm^2 and 0.6 mg/cm^2 Pt on the anode and cathode, respectively. The catalyst coated membrane has a carbon black catalyst support with a surface area of approximately 300 cm^2. To distribute gas from the flow fields to the active area of the membrane, double-sided, hydrophobic, version 3 ETek^{TM} Elats with a thickness of approximately 0.432 mm are used. The flow fields are comprised of machined graphite plates.

9 Parameter Identification Approach

Lacking a practical experimental means to measure the spatial distribution of water mass in the electrodes of a large multi-cell stack, the lumped-parameter two-phase flow model developed here can be indirectly validated through model prediction of the effects of flooding on stack voltage. We concentrate on model parameterization during anode flooding events. Specific operating conditions can be tested for conditions leading to cathode flooding. However, at moderate current densities (< 0.5 A/cm^2) and cell operating temperatures ($\approx 60^o$ C) along with the absence of humidification introduced in the hydrogen gas stream, back diffusion dominates drag, resulting in anode flooding. The accumulation of liquid water in the gas channel and diffusion layer on the anode is typically the dominant reason for voltage degradation. The occurrence of anode flooding is experimentally confirmed by a purging event; following an anode purge, the voltage significantly recovers. Under the same testing conditions and

Copyright © 2005 by ASME

voltage degradation, surging the cathode has little effect on the cell voltages.

Once anode flooding occurs, we postulate that the resulting voltage degradation arises from the accumulation of liquid mass in the GDL, $m_{l_{an}}(3)$ (found from the liquid water mass flow in Equation (19)). The accumulated liquid mass is assumed to form a thin film (experimentally measured in [3]), blocking part of the active fuel cell area A_{fc} and consequently increasing the lumped current density, defined as apparent current density i_{app}:

$$i_{app} = I_{st}/A_{app} \qquad (35)$$

where the apparent fuel cell area A_{app} is approximated as

$$A_{app} = A_{fc}(1 - m_{l_{an}}(3)/(n_{cells}\rho_l t_{wl} A_{fc})) . \qquad (36)$$

The second parameter, α_w, corresponds to the lumped "stack"-level membrane diffusion that needs to be identified using experimental data. The liquid film thickness t_{wl} and the diffusion multiplier α_w are the tunable parameters which are identified by comparing the predicted and measured average cell voltage. A selected section of one experiment is used to identify the two parameters using a nonlinear least squares fitting technique that minimizes the difference between the measured cell voltage, $\bar{v}_{fc}$, and the modeled cell voltage, $\hat{v}_{fc}$,

$$J = \int^{t_{exp}} (\bar{v}_{fc}(\tau) - \hat{v}_{fc}(\tau))^T (\bar{v}_{fc}(\tau) - \hat{v}_{fc}(\tau)) d\tau . \qquad (37)$$

The modeled cell voltage, described in [8], is calculated from

$$\hat{v}_{fc} = E - [v_o + v_a(1 - exp^{-c_1 i_{app}})] - i_{app} R_{ohm} - \left[i_{app} \left(c_2 \frac{i_{app}}{i_{max}} \right)^{c_3} \right]$$

$$= f(p_{H_2,mb}, p_{O_2,mb}, T_{st}, \lambda_{mb}, i_{app})$$

$$(38)$$

where the model parameters were experimentally tuned for a high pressure fuel cell stack.

10 Model Validation Results

Experimental data were collected for a range of stack current from I_{st}=30-90 Amps, air stoichiometries of 200%-300%, coolant circulation temperatures from 50-65°C, at an anode inlet pressure of 1.2 bar. Experimental data and model predictions are shown in Figures 7-10. The data collected for model validation are different from the data used for calibration. Figure 7 shows the model inputs. In particular, subplot 1 shows the total current drawn from the stack I_{st}. The shifted inlet anode and cathode measured pressures ($p_{an,ch}(t) - p_{an,ch}(t = 0)$ and $p_{ca,ch}(t) - p_{ca,ch}(t = 0)$) are shown in subplot 2. All initial values are shown in Table 1. Similarly, the shifted dry air and hydrogen inlet mass flows are shown in subplot 3. The pressure and flow excursions observed in the anode occur after an anode purge is initiated. The purge is scheduled every 180 seconds for 3 seconds. The air mass flow in the cathode inlet, $W_{ca,in}$, was controlled at 300% stoichiometry for this experiment. Finally, the coolant temperature out of the stack is shown in subplot 4. The coolant temperature is regulated thermostatically through a heat

Table 1. Initial values for pressures and flows

Variable	Units	Figure 7	Figure 9
$p_{ca,ch}(0)$	(kPa)	104.59	101.88
$p_{an,ch}(0)$	(kPa)	120.60	120.84
$W_{ca,in}(0)$	(mg/s)	1829.1	292.76
$W_{an,in}(0)$	(mg/s)	20.015	4.3987

exchanger by an on-off fan around a desired set-point. After 57 seconds the desired set point was set from 50°C to 60°C and the stack heats up under its load.

Figure 8 shows the average current density, $i = I_{st}/A_{fc}$, that is used to calculate the molar flux gradients in the GDL next to the catalyst in (13)-(14). The dashed line in the same subplot corresponds to the calculated apparent current density, i_{app}, in (35) based on the apparent area (36) that is not blocked by the liquid water film. The apparent current density is used to calculate the cell overpotential. Subplot 2 shows the measured cell voltages for all 24 cells in the stack (thin lines) and the predicted model voltage (thick line). It is clear that when the apparent current density increases, the predicted voltage decreases matching the measured cell voltages.
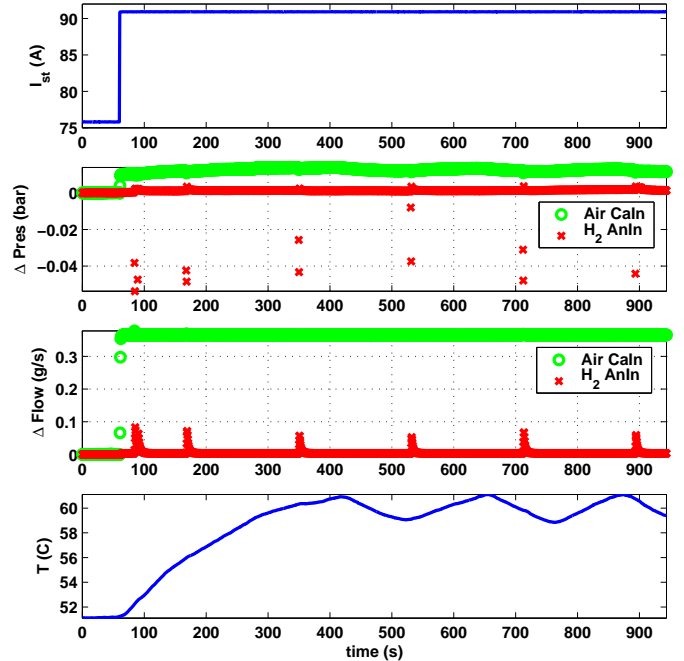

Figure 7. Measurements used as model inputs for one experiment that exhibits anode flooding

Although the voltage prediction is an indirect means for evaluating the overall predictive ability of our model, voltage is a stack variable that combines the internal states of the stack

and provides an accessible, cheap, fast and accurate measurement. The model presented predicts the increase in liquid volume $V_{l,an/ca}$ that consequently decreases reactant diffusion, followed by an increase of the blocked active area, in turn increasing the apparent current density, finally reflected in a decrease in cell voltage. The model accurately captures the trend of the voltage recovery after an anode purging event. Moreover the model predicts the increase in overpotential during a step change in current from 75 to 90 A in the beginning of the experiment. Although the flooding trend is captured, the offset at 90 Amps needs to be addressed with a better voltage parameterization. Note that in [8], the voltage equation underpredicts the measured voltage at high current density. For all experiments conducted, the maximum error in the estimated voltage was found to be 8%.

It is noteworthy that the predicted voltage shows the effects of (a) the instantaneous increase in current (static function) and (b) the excursion in partial pressure of oxygen due to the manifold filling dynamics as indicated by the voltage overshoot during the current step. Finally the model predicts the effects of temperature in the voltage as shown during the temperature transient from 50° to 60^oC. Higher temperature improves the cell voltage through the static polarization function. At the same time, increase in temperature helps evaporate some of the stored liquid as indicated when the apparent current density is equal to the average current density. Consequently, temperature affects the voltage through a dynamic path.
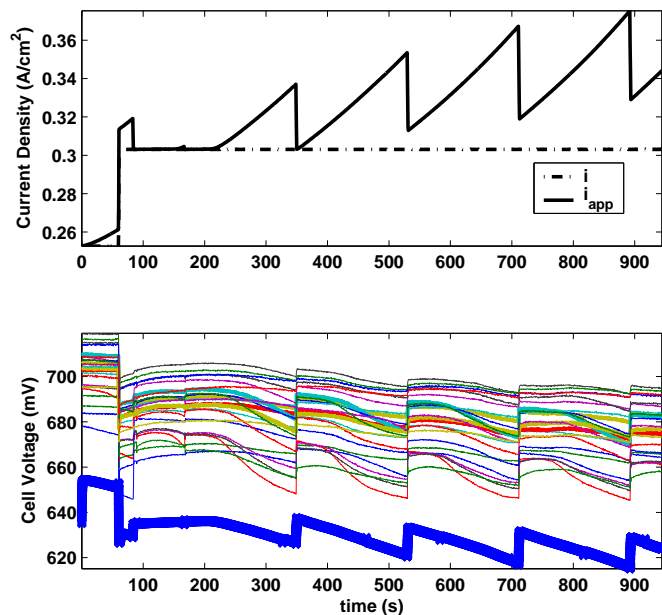

Figure 8. Measurements and model outputs for an experiment exhibiting anode flooding. The thin voltage lines correspond to the measured voltages, the thick line is the model prediction

An additional set of experimental data and model predictions are provided in Figures 9-10. The data shown demonstrate the model predicting capability at low current density and a different range of operating temperature and air stoichiometry. Figure 9 shows the model inputs and Figure 10 shows the average and apparent current density together with the predicted and measured cell voltages. This experiment was completed at I_{st}=30 Amps, 200% air stoichiometry, and a coolant temperature of T_{st}=50° C for the majority of the time. As Figure 10 shows, the model predicts the transient and steady-state voltage during step changes in current, and correctly predicts no significant flooding.
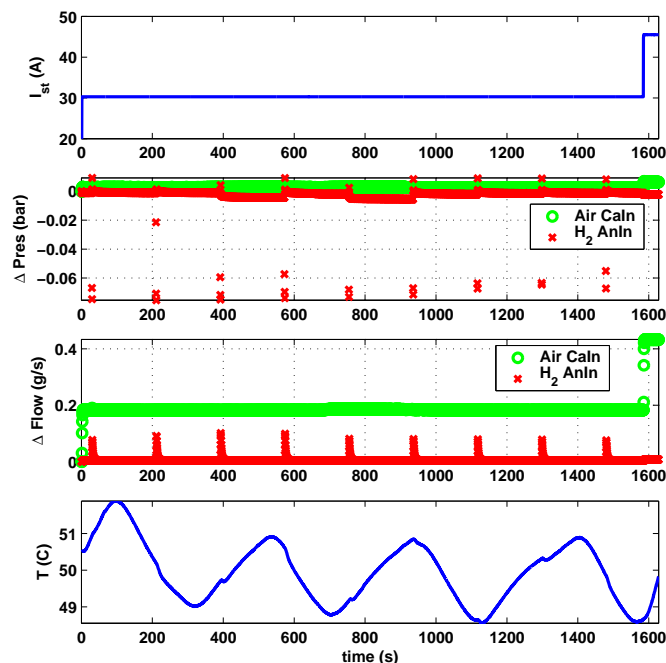

Figure 9. Measurements used as model inputs for an experiment that does not exhibit anode flooding

11 Conclusions

A two-phase one-dimensional model for a multi-cell stack has been developed and validated using experimental transient data. The lumped parameter model depends on two tunable parameters that have been experimentally identified. The model captures dynamics associated with oxygen starvation typically observed during step changes in current demand. Most importantly, the model captures the dynamics associated with two-phase flow through the GDL during electrode flooding or drying.

REFERENCES

[1] Kim, H., Ha, T., Park, S., Min, K., and M.S.Kim, 2005. "Visualization study of cathode flooding with different operating conditions in a pem unit fuel cell". Proceedings of
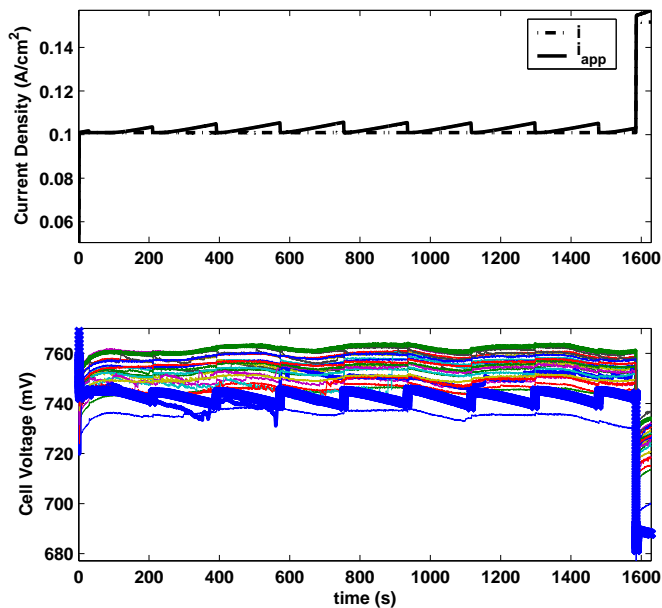
Figure 10.   Measurements and model outputs for an experiment that does not exhibit anode flooding. The thin voltage lines correspond to the measured voltage of the 24 cells and the thick line is the model calculation

Fuel Cell 2005, ASME Conference on Fuel Cell Science, Engineering and Technology.

[2] Hickner, M., and Chen, K., 2005. "Experimental studies of liquid water droplet growth and instability at the gas diffusion layer/gas flow channel interface". Proceedings of Fuel Cell 2005, ASME Conference on Fuel Cell Science, Engineering and Technology.

[3] Chuang, P.-Y. A., Turhan, A., Heller, A. K., Brenizer, J. S., Trabold, T. A., and Mench, M., 2005. "The nature of flooding and drying in polymer electrolyte fuel cells". Proceedings of Fuel Cell 2005, ASME Conference on Fuel Cell Science, Engineering and Technology.

[4] Yi, J., and Nguyen, T., 1998. "An along the channel model for proton exchange membrane fuel cells". *Journal of the Electrochemical Society,* **145**(4).

[5] Fuller, T., and Newman, J., 1993. "Water and thermal management in solid-polymer-electrolyte fuel cells". *Journal of the Electrochemical Society,* **140**(5).

[6] S. Dutta, S. S., and Zee, J. V., 2001. "Numerical prediction of mass-exchange between cathode and anode channels in a pem fuel cell". *International Journal of Heat and Mass Transfer,* **44**, pp. 2029–2042.

[7] Pasaogullari, U., and Wang, C.-Y., 2005. "Two-phase modeling and flooding prediction of polymer electrolyte fuel cells". *Journal of the Electrochemical Society,* **152**(2).

[8] Pukrushpan, J. T., Stefanopoulou, A. G., and Peng, H., 2000. *Control of Fuel Cell Power Systems: Principles,*

Modeling, Analysis and Feedback Design. Springer, New York.

[9] Fuller, T. F., 1992. "Solid polymer-electrolyte fuel cells". PhD thesis, University of California, Berkeley.

[10] Springer, T., Zawodzinski, T., and Gottesfeld, S., 1991. "Polymer electrolyte fuel cell model". *Journal of the Electrochemical Society,* **138**.

[11] Motupally, S., Becker, A., and Weidner, J., 2000. "Diffusion of water in nafion 115 membranes". *Journal of The Electrochemical Society,* **147**(9).

[12] Nam, J. H., and Kaviany, M., 2003. "Effective diffusivity and water-saturation distribution in single- and two-layer pemfc diffusion medium". *Int. J Heat Mass Transfer,* **46**, pp. 4595–4611.

[13] Hanamura, K., and Kaviany, M., 1995. "Propagation of condensation front in steam injection into dry porous media". pp. 1377–1386.

[14] Lydersen, A. L., 1983. *Mass Transfer in Engineering Practice.* John Wiley & Sons, New York.

[15] Kaviany, M., 1999. *Principles of Heat Transfer in Porous Media, second ed.* Springer, New York.